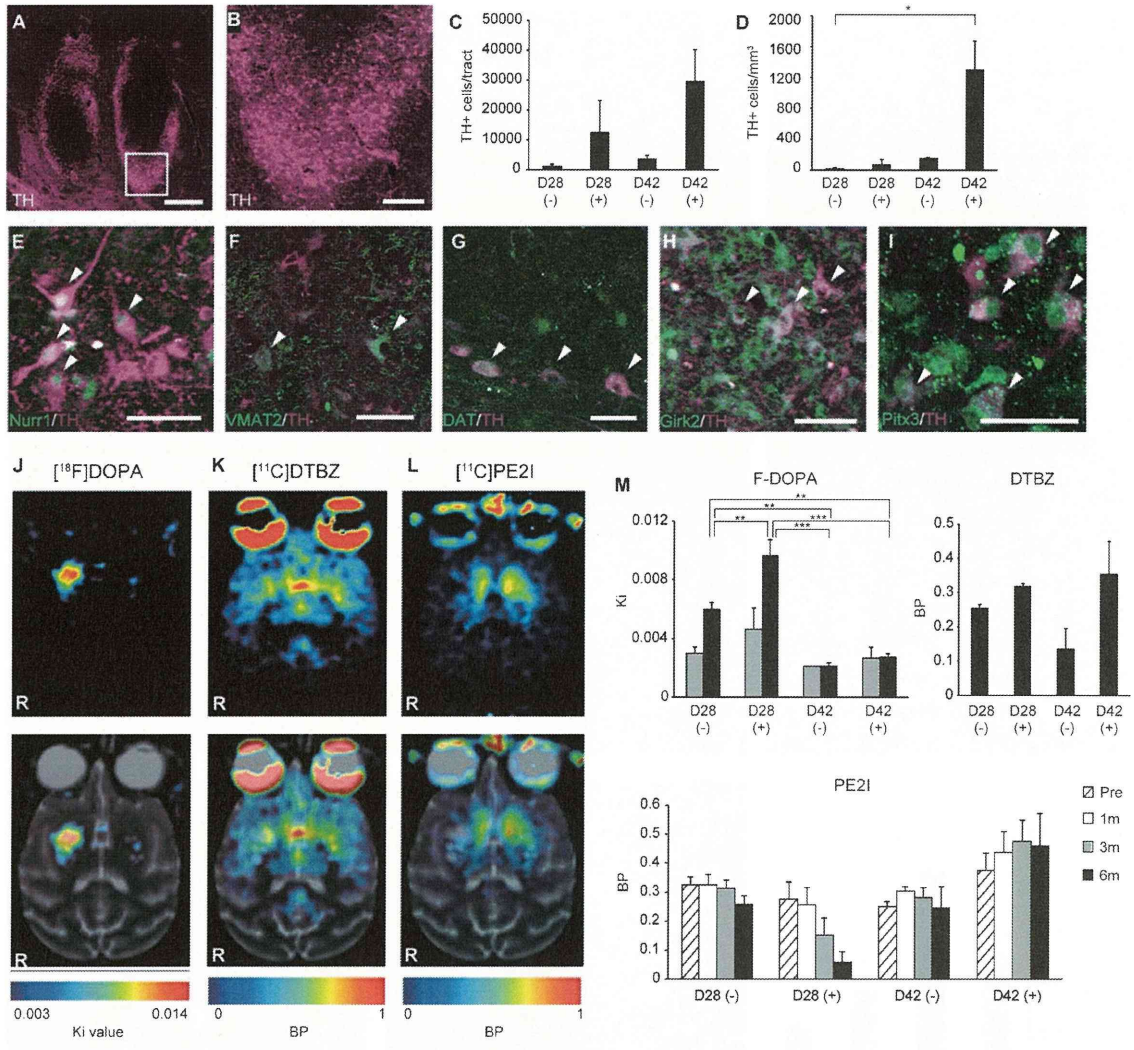

Fig. 5. DA neuron differentiation from grafted NPCs in a monkey brain. (A, B) Immunofluorescence images of d42 grafts stained for TH at 6 months after transplantation. A magnified image of the area denoted in (A) is shown in (B). Scale bars, 1 mm in (A) and 200 μm in (B). (C) The number of TH^+ cells/graft, and (D) number of TH^+ cells/mm^3 are presented as means ± SEM. (*$P < 0.05$, ANOVA) (E–I) Immunofluorescence images showing labeling of TH (magenta) and Nurr1 (green in E), VMAT2 (green in F), DAT (green in G), Girk2 (green in H), or Pitx3 (green in I). Scale bars, 50 μm. (J–L) T2-weighted magnetic resonance images with overlapping data obtained using [^{18}F]DOPA-PET (J), [^{11}C]DTBZ-PET (K), or [^{11}C]PE2I-PET (L) at 6 months after transplantation. (M) Ki values ([^{18}F]DOPA) and binding potentials ([^{11}C]DTBZ, [^{11}C]PE2I) at the indicated time points are presented as means ± SEM (*$P < 0.05$, **$P < 0.01$, ***$P < 0.001$, ANOVA).

cells were less tumorigenic as the differentiation period increased [21]. The proliferating NPCs in the d28 spheres also generated TH^+ cells in the graft, whereas TH^+ cells in d42 spheres did not survive in the mouse brains probably because of issues related to xenografts between human and mice.

In contrast to the mouse studies, d42 spheres generated a substantial number of DA neurons in the monkey brain. Furthermore, treatment with Shh and FGF8 followed by BDNF and GDNF was required to generate mature DA neurons. As discussed above, d28 spheres that resulted in continuous proliferation of $Vimentin^+$ and $Nestin^+$ cells were too immature to generate mature DA neurons in the brain when such neurotrophic factors as BDNF and GDNF were absent. These results are consistent with

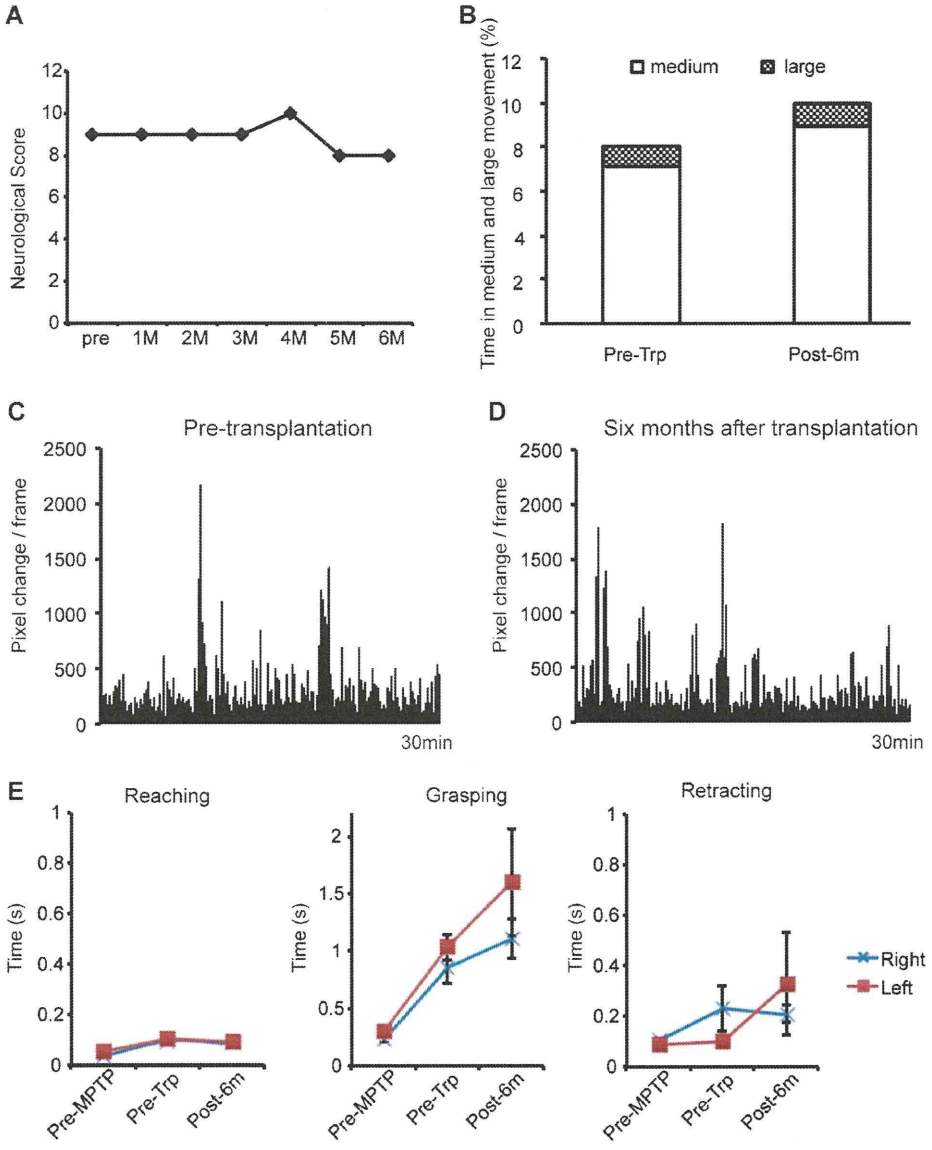

Fig. 6. Neurologic function in an MPTP-treated monkey. (A) Neurologic scores for the monkey before and after cell transplantation. (B) Percentage of time spent making medium or large movements before and 6 months after transplantation. The rest of the time was spent making small movements. (C, D) Pixel changes in each 66.67-ms time period based on spontaneous movements of the monkey during a 30-min trial. (E) Time spent reaching, grasping, and retracting in a raisin pick-up test. Data are presented as the means ± SEM ($P > 0.05$, Student's t test).

previous studies showing good survival of DA neurons in allografts derived from mouse embryonic stem cells [12] and monkey embryonic tissues [22] undergoing neurogenesis into DA neurons. Intriguingly, d28 spheres treated with Shh and FGF8 produced larger grafts, which may reflect maintenance of $Pax6^+$ rosette-forming neuroepithelial cells by Shh and FGF8 [23]. Yet even d42 spheres did not provide a perfect donor population, because some $Nestin^+$ cells were still proliferating in the core of the graft 6 months after transplantation. Therefore, safer and more efficient transplantation will require some modification of our approach, such as purifying DA neuron progenitors or promoting DA maturation *in vivo*.

PET has been extensively employed to elucidate functional changes associated with PD, and [^{18}F]DOPA-PET is the gold standard for assessing dopamine synthesis. In this study, however, uptake of [^{18}F]DOPA was much greater in d28 grafts even though they contained only a small number of TH$^+$ cells. The observed uptake may have reflected accumulation of OMFD, a major metabolite of [^{18}F]DOPA that penetrates the blood–brain barrier and accumulates in brain tumors [24]. Thus, high levels of [^{18}F]DOPA uptake in d28 grafts may indicate cell proliferation rather than dopamine synthesis, a particularly relevant consideration for stem cell transplantation. As demonstrated in this study, examining ligands for dopamine synthesis, transport, and reuptake reflects DA activity in the grafted NPCs. Furthermore, these approaches can also be used in human patients.

Patients with PD who received fetal cell grafts required at least 100,000 TH$^+$ cells in each putamen to achieve good clinical responses [5]. Because the monkey putamen is one-tenth the size of the human putamen [25, 26], we estimated that 10,000 cells were needed for a monkey to recover from neurologic deterioration. Thus, the d42 grafts in this study should have contained a sufficient number of TH$^+$ cells (150,000 in total). Furthermore, some of the TH$^+$ cells that were located in the periphery region expressed Pitx3$^+$ and Girk2$^+$, suggesting that they were A9 DA neurons and able to innervate striatum [27]. Behavioral improvements, however, were moderate in this study. This may reflect insufficient maturation of the majority of TH$^+$ cells or differentiation to an inappropriate fate (namely, into diencephalic or olfactory bulb DA neurons). The follow-up period post-transplantation may have been too short to allow the human neurons to functionally integrate into the brain. Alternatively, functional synapses may not form well in this xeno-transplantation model. Finally, the remaining NPCs or other cell types in the graft (e.g., GABA neurons) may have suppressed the function of the iPSC-derived DA neurons.

In conclusion, we have successfully induced the development of DA neurons using a feeder-free culture method. Moreover, the cells survived for 6 months in the brain of a primate PD model. A substantial number of DA neurons were obtained from d42 spheres treated with Shh and FGF8 followed by BDNF and GDNF. We also developed a system to evaluate the transplanted cells using MRI and PET, behavioral analyses, and histologic examinations, all of which will be useful in preclinical research. Additional studies using other primate models and NPCs subjected to alternative pretreatment protocols will help elucidate the therapeutic potential of human iPSCs.

ACKNOWLEDGMENTS

We thank Drs. K. Takahashi and S. Yamanaka (Kyoto University, Center for iPS Cell Research and Application) for providing human iPSCs, Dr. Y. Ono (KAN Research Institute) for anti-Nurr1 antibodies, Drs. T. Yamamoto and H. Magotani (Shin Nippon Biomedical Laboratories) for their help with the monkey, Astellas Pharma for FK506, and Mr. K. Kubota and Ms. M. Katsukawa in our laboratory for their technical assistance. This study was supported by the following grants: a grant from the Project for Realization of Regenerative Medicine from the MEXT, and a Health and Labor Sciences Research Grant for Research on Regenerative Medicine for Clinical Application. The authors declare that they have no competing interests.

REFERENCES

[1] Wernig M, Zhao JP, Pruszak J, Hedlund E, Fu D, Soldner F, Broccoli V, Constantine-Paton M, Isacson O, & Jaenisch R (2008) Neurons derived from reprogrammed fibroblasts functionally integrate into the fetal brain and improve symptoms of rats with Parkinson's disease. *Proc Natl Acad Sci U S A*, **7**, 7.

[2] Hargus G, Cooper O, Deleidi M, Levy A, Lee K, Marlow E, Yow A, Soldner F, Hockemeyer D, Hallett PJ, Osborn T, Jaenisch R, & Isacson O (2010) Differentiated Parkinson patient-derived induced pluripotent stem cells grow in the adult rodent brain and reduce motor asymmetry in Parkinsonian rats. *Proc Natl Acad Sci U S A*, **107**, 15921-15926.

[3] Freed CR, Greene PE, Breeze RE, Tsai WY, DuMouchel W, Kao R, Dillon S, Winfield H, Culver S, Trojanowski JQ, Eidelberg D, & Fahn S (2001) Transplantation of embryonic dopamine neurons for severe Parkinson's disease. *N Engl J Med*, **344**, 710-719.

[4] Olanow CW, Goetz CG, Kordower JH, Stoessl AJ, Sossi V, Brin MF, Shannon KM, Nauert GM, Perl DP, Godbold J, & Freeman TB (2003) A double-blind controlled trial of bilateral fetal nigral transplantation in Parkinson's disease. *Ann Neurol*, **54**, 403-414.

[5] Lindvall O, & Björklund A (2004) Cell therapy in Parkinson's disease. *NeuroRx*, **1**, 382-393.

[6] Takagi Y, Takahashi J, Saiki H, Morizane A, Hayashi T, Kishi Y, Fukuda H, Okamoto Y, Koyanagi M, Ideguchi M, Hayashi H, Imazato T, Kawasaki H, Suemori H, Omachi S, Iida H, Itoh N, Nakatsuji N, Sasai Y, & Hashimoto N (2005) Dopaminergic neurons generated from monkey embryonic stem cells function in a Parkinson primate model. *J Clin Invest*, **115**, 102-109.

[7] Sanchez-Pernaute R, Studer L, Ferrari D, Perrier A, Lee H, Vinuela A, & Isacson O (2005) Long-term survival of dopamine neurons derived from parthenogenetic primate embryonic stem cells (cyno-1) after transplantation. *Stem Cells*, **23**, 914-922.

[8] Redmond DEJ, Bjugstad KB, Teng YD, Ourednik V, Ourednik J, Wakeman DR, Parsons XH, Gonzalez R, Blanchard BC, Kim SU, Gu Z, Lipton SA, Markakis EA, Roth RH, Elsworth JD, Sladek JRJ, Sidman RL, & Snyder EY (2007) Behavioral improvement in a primate Parkinson's model is associated with multiple homeostatic effects of human neural stem cells. *Proc Natl Acad Sci U S A*, **104**, 12175-12180.
[9] Takahashi K, Tanabe K, Ohnuki M, Narita M, Ichisaka T, Tomoda K, & Yamanaka S (2007) Induction of pluripotent stem cells from adult human fibroblasts by defined factors. *Cell*, **131**, 861-872.
[10] Watanabe K, Ueno M, Kamiya D, Nishiyama A, Matsumura M, Wataya T, Takahashi JB, Nishikawa S, Muguruma K, & Sasai Y (2007) A ROCK inhibitor permits survival of dissociated human embryonic stem cells. *Nat Biotechnol*, **25**, 681-686.
[11] Koyanagi M, Takahashi J, Arakawa Y, Doi D, Fukuda H, Hayashi H, Narumiya S, & Hashimoto N (2008) Inhibition of the Rho/ROCK pathway reduces apoptosis during transplantation of embryonic stem cell-derived neural precursors. *J Neurosci Res*, **86**, 270-280.
[12] Morizane A, Doi D, Kikuchi T, Nishimura K, & Takahashi J (2011) Small-molecule inhibitors of bone morphogenic protein and activin/nodal signals promote highly efficient neural induction from human pluripotent stem cells. *J Neurosci Res*, **89**, 117-126.
[13] Smith SM, Jenkinson M, Woolrich MW, Beckmann CF, Behrens TE, Johansen-Berg H, Bannister PR, De Luca M, Drobnjak I, Flitney DE, Niazy RK, Saunders J, Vickers J, Zhang Y, De Stefano N, Brady JM, & Matthews PM (2004) Advances in functional and structural MR image analysis and implementation as FSL. *Neuroimage*, **23**(Suppl 1), S208-S219.
[14] Smith SM (2002) Fast robust automated brain extraction. *Hum Brain Mapp*, **17**, 143-155.
[15] Jenkinson M, & Smith S (2001) A global optimisation method for robust affine registration of brain images. *Med Image Anal*, **5**, 143-156.
[16] Zhang Y, Brady M, & Smith S (2001) Segmentation of brain MR images through a hidden Markov random field model and the expectation-maximization algorithm. *IEEE Trans Med Imaging*, **20**, 45-57.
[17] Saiki H, Hayashi T, Takahashi R, & Takahashi J (2010) Objective and quantitative evaluation of motor function in a monkey model of Parkinson's disease. *J Neurosci Methods*, **190**, 198-204.
[18] Saga T, Kawashima H, Araki N, Takahashi JA, Nakashima Y, Higashi T, Oya N, Mukai T, Hojo M, Hashimoto N, Manabe T, Hiraoka M, & Togashi K (2006) Evaluation of primary brain tumors with FLT-PET: Usefulness and limitations. *Clin Nucl Med*, **31**, 774-780.
[19] Poyot T, Condé F, Grégoire MC, Frouin V, Coulon C, Fuseau C, Hinnen F, Dollé F, Hantraye P, & Bottlaender M (2001) Anatomic and biochemical correlates of the dopamine transporter ligand 11C-PE2I in normal and parkinsonian primates: Comparison with 6-[18F]fluoro-L-dopa. *J Cereb Blood Flow Metab*, **21**, 782-792.
[20] Pavese N, & Brooks DJ (2009) Imaging neurodegeneration in Parkinson's disease. *Biochim Biophys Acta*, **1792**, 722-729.
[21] Brederlau A, Correia AS, Anisimov SV, Elmi M, Paul G, Roybon L, Morizane A, Bergquist F, Riebe I, Nannmark U, Carta M, Hanse E, Takahashi J, Sasai Y, Funa K, Brundin P, Eriksson PS, & Li JY (2006) Transplantation of human embryonic stem cell-derived cells to a rat model of Parkinson's disease: Effect of *in vitro* differentiation on graft survival and teratoma formation. *Stem Cells*, **24**, 1433-1440.
[22] Elsworth JD, Sladek JR, Taylor JR, Collier TJ, Redmond DE, & Roth RH (1996) Early gestational mesencephalon grafts, but not later gestational mesencephalon, cerebellum or sham grafts, increase dopamine in caudate nucleus of MPTP-treated monkeys. *Neuroscience*, **72**, 477-484.
[23] Elkabetz Y, Panagiotakos G, Al Shamy G, Socci ND, Tabar V, & Studer L (2008) Human ES cell-derived neural rosettes reveal a functionally distinct early neural stem cell stage. *Genes Dev*, **22**, 152-165.
[24] Beuthien-Baumann B, Bredow J, Burchert W, uuml F, chtner F, Bergmann R, Alheit HD, Reiss G, Hliscs R, Steinmeier R, Franke WG, Johannsen B, & Kotzerke J (2003) 3-O-methyl-6-[18F]fluoro-L-DOPA and its evaluation in brain tumour imaging. *Eur J Nucl Med Mol Imaging*, **30**, 1004-1008.
[25] Schaltenbrand G, & Wahren W (1997) Atlas for stereotaxy of the human brain, Georg Thieme Verlag, Stuttgart, Germany, plate 17, a.13.5-p.1.5.
[26] Martin RF, & Bowden DM (2000) Primate Brain Maps: Structure of the Macaque Brain, Elsevier Science Ltd, 270-284.
[27] Thompson L, Barraud P, Andersson E, Kirik D, & Bjorklund A (2005) Identification of dopaminergic neurons of nigral and ventral tegmental area subtypes in grafts of fetal ventral mesencephalon based on cell morphology, protein expression, and efferent projections. *J Neurosci*, **25**, 6467-6477.

SUPPLEMENTARY METHODS

MRI scans

Before transplantation, a high-resolution T1-weighted image was obtained for each animal using a fast spoiled gradient-echo (FSPGR) sequence (TR = 7.812 ms, TE = 1.912 ms, TI = 600 ms, FA = 7°, matrix = 128 × 128, field of view (FOV) = 102.4 mm, slice thickness = 0.8 mm), and examined to identify the injection site (posterodorsal striatum) in the grafts. After transplantation, T1-weighted, T2-weighted, and fluid-attenuated-inversion recovery (FLAIR) images were obtained with thicker slices and used to evaluate brain pathology qualitatively with a better signal-to-noise ratio. T1 images were obtained using an FSPGR sequence (TR = 7.504 ms, TE = 1.784 ms, TI = 600 ms, FA = 7°, matrix = 128 × 128, FOV = 100 mm, slice thickness = 2 mm), T2 images were obtained using a fast spin echo sequence (TR = 5400 ms, TE = 101.024, FA = 90°, matrix = 160 × 160, FOV = 100 mm, slice thickness = 2 mm), and FLAIR image were obtained using an inversion recovery sequence (TR = 8502 ms, TE = 83.22 ms, IR = 2800 ms, FA = 90°, matrix = 160 × x160, FOV = 100 mm, slice thickness = 2 mm).

Preparation of PET ligands

[^{11}C]PE2I was prepared by exposing the corresponding free acid precursor (1.2 mg) in

Supplementary Table 1
Real-time RT-PCR primers

Gene Name	Forward	Reverse
Oct3/4	5′- CCCCAGGGCCCCATTTTGGTACC-3′	5′-ACCTCAGTTTGAATGCATGGGAGAGC-3′
Nanog	5′-GGCTCTGTTTTGCTATATCCCCTAA-3′	5′-CATTACGATGCAGCAAATACGAGA-3′
Sox2	5′-TTCACATGTCCCAGCACTACCAGA-3′	5′-TCACATGTGTGAGAGGGGCAGTGTGC-3′
Klf4	5′-CATGCCAGAGGAGCCCAAGCCAAAGAGGGG-3′	5′-CGCAGGTGTGCCTTGAGATGGGAACTCTTT-3′
cMyc	5′-ATACATCCTGTCCGTCCAAGCAGA-3′	5′-ACGCACAAGAGTTCCGTAGCTG-3′
Sox1	5′-GCGGAGCTCGTCGCATT-3′	5′-GCGGTAACAACTACAAAAAACTTGTAA-3′
Pax6	5′-CTGGCTAGCGAAAAGCAACAG-3′	5′-CCCGTTCAACATCCTTAGTTTATCA-3′
TH	5′-GCAGTTCTCGCAGGACATTG-3′	5′-CGGCACCATAGGCCTTCA-3′
β-actin	5′-CACCATTGGCAATGAGCGGTTC-3′	5′-CACCATTGGCAATGAGCGGTTC-3′

Supplementary Table 2
Primary antibodies used for immunofluorescence studies

Antibody	Dilution	Company
mouse anti-Oct3	1 : 100	Santa Cruz Biotechnology
rabbit anti-TH	1 : 200	Millipore Chemicon
mouse anti-TH	1 : 200	Millipore Chemicon
mouse anti-Tuj1	1 :100	Millipore Chemicon
mouse anti-Nestin	1 : 300	Covance Research Products
rat anti-DAT	1 : 1000	Millipore Chemicon
mouse anti-Pax6	1 : 500	Hybridoma Bank
rabbit anti-Pax6	1 : 200	Covance Research Products
rat anti-Nurr1	1 : 1000	A gift from KAN laboratory
rabbit anti-Ki67	1 : 1000	Novocastra
rabbit anti-Girk2	1 : 100	Alomone Labs
rabbit anti-VMAT2	1 : 400	Pel-Freez
goat anti-Nanog	1 : 200	R&D
mouse anti-Vimentin	1 : 500	Millipore Chemicon

dimethylformamide (400 μl) to [^{11}C]-CH_3I produced in a cyclotron (HM12; Sumitomo Heavy Industry, Tokyo, Japan). Precursor and standard PE2I were purchased from PharmaSynth AS (Tartu, Estonia). Radiochemical purities were greater than 95%, and specific activities were 63.8 ± 6.8 GBq/μmol (mean ± SEM) at the time of injection. [^{11}C]DTBZ was prepared by exposing (+)-9-O-desmethyl-α-dihydrotetrabenazine (DTBZ precursor) (0.8 mg) in anhydrous dimethyl sulfoxide (400 μl) to [^{11}C]-CH_3I. Precursor and standard DTBZ were purchased from ABX (Radeberg, Germany). Radiochemical purities were greater than 99.5%, and specific activities were greater than 72.6 GBq/μmol at the time of injection.

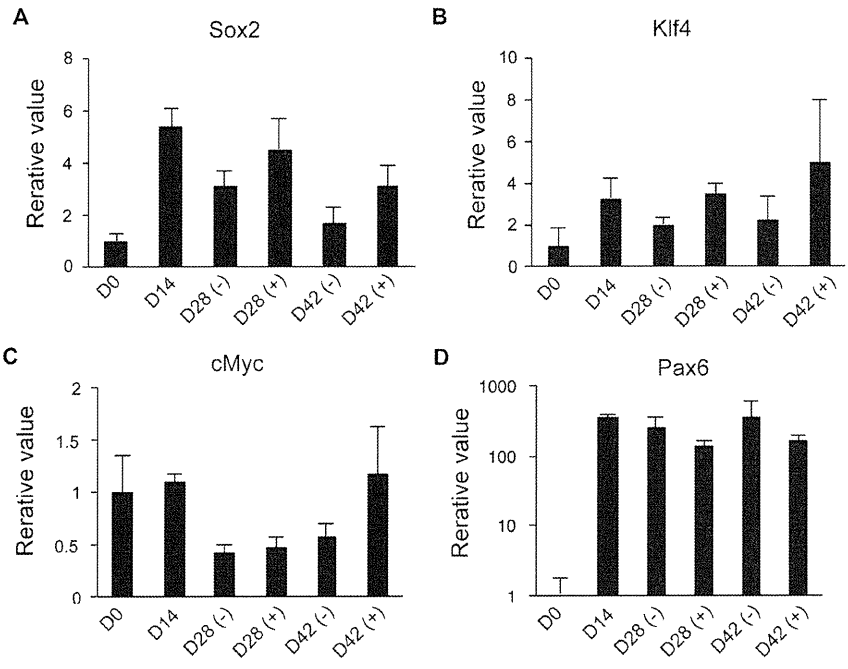

Supplementary Figure 1. Quantitative RT-PCRs to examine the expression of *Sox2* (A), *Klf4* (B), *c-Myc* (C), and *Pax6* (D) in human iPSC-derived spheres.

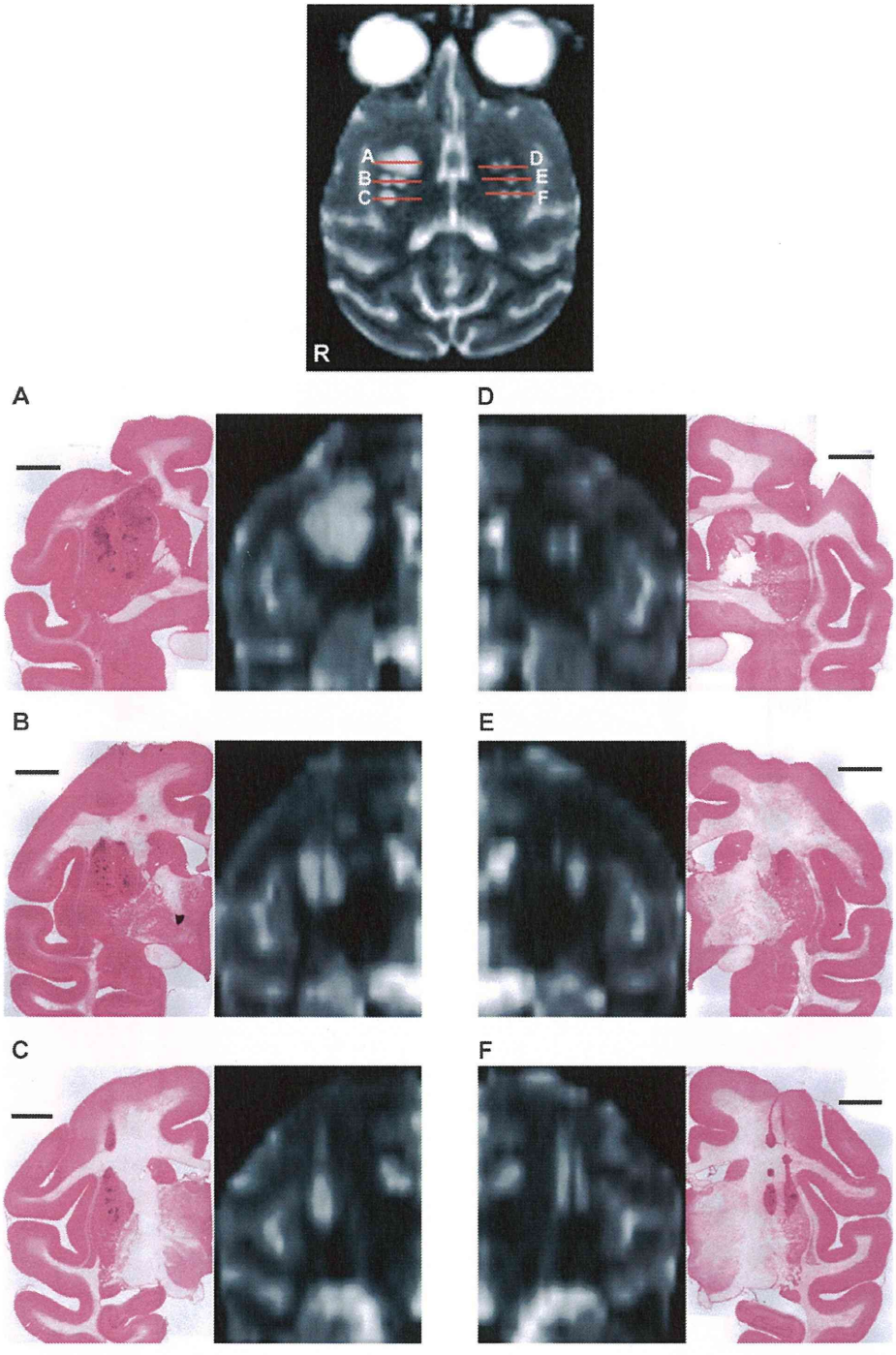

Supplementary Figure 2. A reconstructed T2-weighted magnetic resonance image and H–E staining of identical brain sections (coronal view). Scale bars, 5 mm.

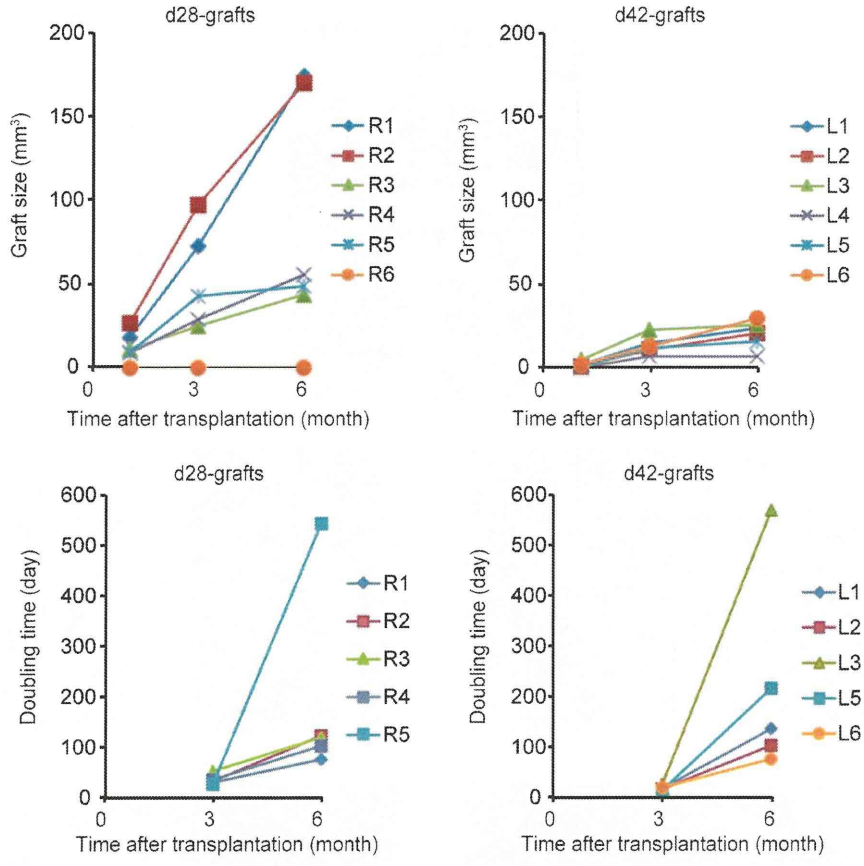

Supplementary Figure 3. Graft size and doubling time in each tract of the iPSC-derived grafts during 1–3 months and 3–6 months post-transplantation. R, right; L, left.

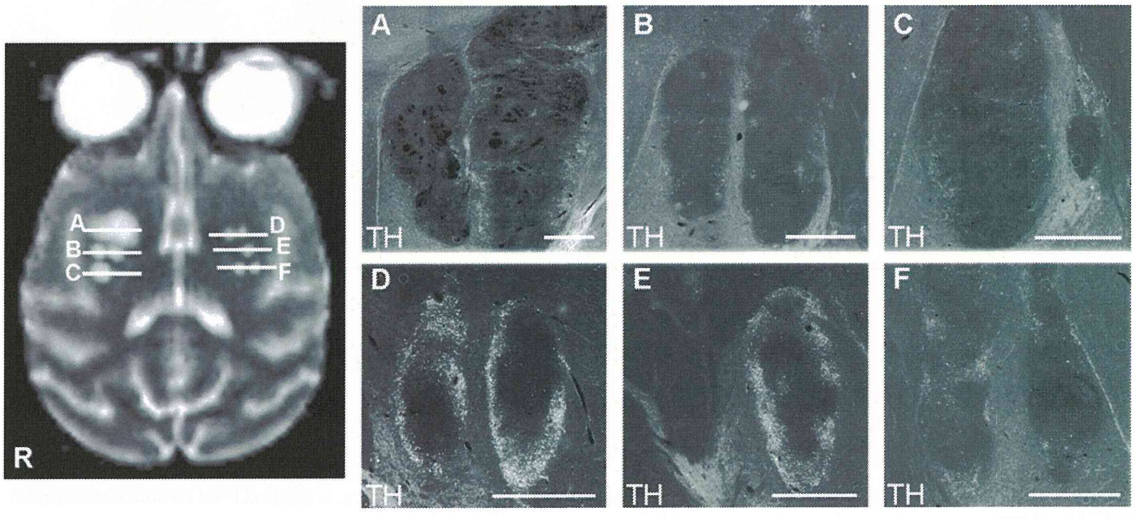

Supplementary Figure 4. Immunofluorescence labeling of tyrosine hydroxylase in each tract of the iPSC-derived grafts 6 months after transplantation. Scale bars, 2 mm. The graphs show the number of TH^+ cells per graft, and per volume (1 mm^3) in each tract.

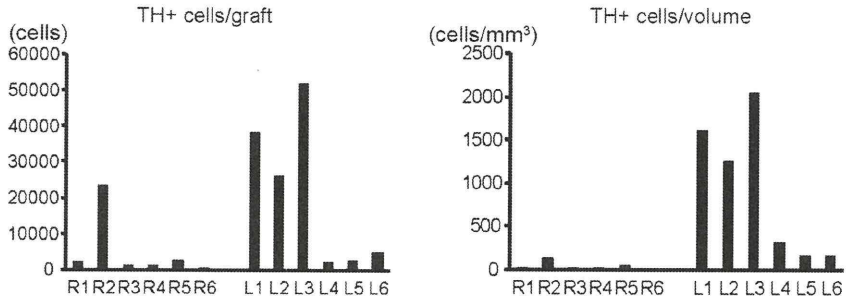

Supplementary Figure 4. (*Continued*)

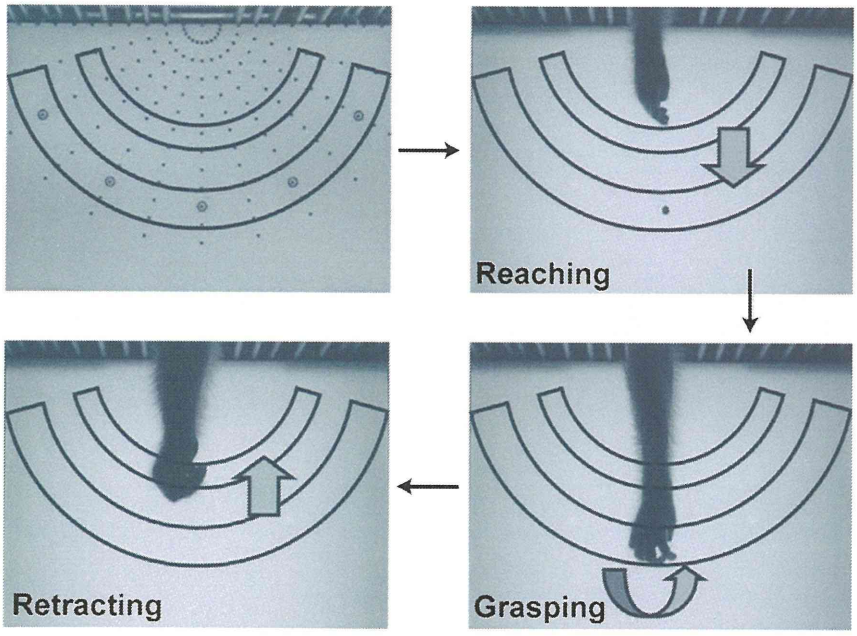

Supplementary Figure 5. Raisin pick-up test. We assessed the time it took for the monkey's hand to move from the first area to the second area (reaching), from the second area to grasp the raisin (grasping), and from the second area to the first area (retracting).

[^{18}F]DOPA and [^{18}F]FLT were synthesized according to previously reported procedures [1, 2].

PET image analysis

[^{18}F]FLT 9PET images obtained for 60 min (30–90 min after the injection) were converted into standardized uptake values to analyze [^{18}F]FLT accumulation. To obtain parametric images, PET results were analyzed using suita ble tracer kinetic models and PMOD software version 3.0 (PMOD Technologies, Adliswil, Switzerland). The examined parameters included uptake rate (Ki, min^{-1}) for [^{18}F]DOPA and the binding potential between the VMAT2 transporter or DA transporter and [^{11}C]DTBZ or [^{11}C]PE2I, respectively. [^{18}F]DOPA Ki was calculated using Patlak graphic analysis, with the cerebellum as the reference region [3]. To quantitate [^{11}C]DTBZ and [^{11}C]PE2I binding in the brain, we calculated binding potentials using the Ichise multilinear reference tissue model [4] and the simplified reference tissue model [5], respectively, with the cerebellum as the reference region. To determine anatomic locations, PMOD software was used to precisely coregister PET and MRI results.

REFERENCES

[1] Ishiwata K, Ishii S-I, Senda M, Tsuchiya Y, & Tomimoto K (1993) Electrophilic synthesis of 6-[18F]fluoro-l-dopa: Use of 4-O-pivaloyl-l-dopa as a suitable precursor for routine production. *Applied Radiation and Isotopes*, **44**, 755-759.

[2] Wodarski C, Eisenbarth J, Weber K, Henze M, Haberkorn U, & Eisenhut M (2000) Synthesis of 3′-deoxy-3′-[18F]fluorothymidine with 2,3′-anhydro-5′-O-(4,4′-dimethoxytrityl)-thymidine. *Journal of Labelled Compounds and Radiopharmaceuticals*, **43**, 1211-1218.

[3] Patlak CS, & Blasberg RG (1985) Graphical evaluation of blood-to-brain transfer constants from multiple-time uptake data Generalizations. *J Cereb Blood Flow Metab*, **5**, 584-590.

[4] Ichise M, Ballinger JR, Golan H, Vines D, Luong A, Tsai S, & Kung HF (1996) Noninvasive quantification of dopamine D2 receptors with iodine-123-IBF SPECT. *J Nucl Med*, **37**, 513-520.

[5] Lammertsma AA, & Hume SP (1996) Simplified reference tissue model for PET receptor studies. *Neuroimage*, **4**, 153-158.